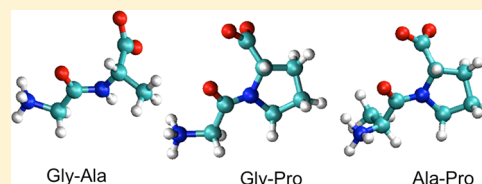


Polarizable Molecular Dynamics Simulations of Aqueous Dipeptides

Tugba G. Kucukkal and Steven J. Stuart*

Department of Chemistry, Clemson University, Clemson, South Carolina 29634, United States

ABSTRACT: Molecular dynamics simulations were carried out for concentrated aqueous solutions of three dipeptides: Gly-Ala, Gly-Pro, and Ala-Pro. The simulations were performed using both polarizable and nonpolarizable force fields, as a method of assessing the effects of polarization in a well-characterized biomolecular system, and to determine whether the models are adequate to reproduce observed aggregation behavior. The structure and dynamics of both solute and solvent were analyzed and the results compared to experiment, including neutron diffraction measurements of peptide aggregation. The polarizable water is depolarized in concentrated peptide solutions, reflecting its ability to adapt to heterogeneous electrostatic environments. Significant differences between the polarizable and nonpolarizable models are found in terms of both the structure and the dynamics of water as a solvent. Although the water shows more realistic structure and dynamics in the polarizable simulations, consistent with enhanced peptide–water interaction, the peptide aggregation behavior agrees less well with the experiment. Neither model successfully reproduces the experimentally observed dipeptide aggregation behavior.



■ INTRODUCTION

The large majority of biomolecular simulations use fixed-charge force fields, in which electrostatic interactions are represented by constant point charges, and any polarization is treated implicitly, through enhanced charges that represent the mean-field polarization response to the aqueous environment. Although this is adequate for many applications, a more accurate treatment of polarization is needed in nonstandard environments, such as in the interior of proteins, in low-polarity solvents, near hydrophobic surfaces, near strongly charged solutes, or for confined water, among other examples.^{1–11} Many polarizable force fields have been developed to address these issues,^{12–34} but their application to biological systems remains relatively limited. Consequently, there continues to be a strong need to assess the effects of polarizability in biomolecular simulations.

Aqueous dipeptide solutions serve as an ideal system for such purposes. The interaction of simple peptides is often used as a proxy for protein hydration, with the assumption that a more complete understanding of the forces driving peptide association will lead to progress in understanding protein folding,^{35–39} given that dynamics of interfacial water seem to drive much of protein folding dynamics.^{40,41} The small size and relatively fast diffusion of the dipeptides makes them amenable to computational study at nanometer length and nanosecond time scales, while their relatively simple structure allows the solutions to be studied by a range of different experimental techniques. However, even though these systems are chosen to mimic aqueous proteins (for which polarizable models are often not needed), the peptide concentrations used to model the environment of a folding protein are often 30 wt % or more. At these concentrations, the majority of the water in the solution is interfacial and may be strongly perturbed by the zwitterionic charges and/or the hydrophobic side chains of one or more

peptides, so it is reasonable to suspect that an explicit treatment of polarization may be important.

Aqueous solutions of the three dipeptides Gly-Ala, Gly-Pro, and Ala-Pro were investigated in this study. These three were chosen because they are amphiphilic, but with a range of hydrophobicities, and all three have been studied experimentally via neutron diffraction.^{37,42} The Gly-Ala dipeptide has been previously studied using the CHARMM22 fixed-charge potential and three different water models, and it was found that the degree of association was considerably underestimated in all of these nonpolarizable simulations.⁴³ In the current study, all three dipeptides were modeled in concentrated aqueous solution using the CHARMM polarizable^{18,19} and fixed-charge⁴⁴ potentials, together with the polarizable TIP4P-FQ¹⁴ and fixed-charge TIP3P^{45,46} water models, respectively. The structure and dynamics of both the peptides and the solvent were evaluated and compared to experiment, to explore the importance of explicit polarization on both peptide–water and peptide–peptide interactions in these concentrated dipeptide solutions.

■ METHODS

Molecular dynamics simulations of Gly-Ala, Gly-Pro, and Ala-Pro solutions were performed using the CHARMM molecular mechanics program.⁴⁷ The TIP4P-FQ¹⁴ and TIP3P^{45,46} water models were used with the polarizable CHARMM30^{18,19} and fixed-charge CHARMM22⁴⁴ force fields for dipeptides, respectively. The CMAP correction^{48,49} was used for all amino acids in the nonpolarizable simulations, and all except proline in the polarizable simulations (for which CMAP proline parameters are not available). All simulations were performed

Received: January 16, 2012

Revised: June 29, 2012

Published: June 30, 2012

in the isothermal–isobaric (*NPT*) ensemble at 298 K and 1 atm. Temperature control was achieved with the Nosé–Hoover thermostat,^{50,51} and pressure control with the Langevin barostat.⁵² The SHAKE algorithm⁵³ was used to constrain bonds between hydrogen and heavy atoms. The leapfrog Verlet algorithm was used to integrate the equations of motion. Time steps of 0.5 and 2 fs were used in the polarizable and fixed-charge simulations, respectively. Cubic simulation boxes with periodic boundary conditions were used with particle mesh Ewald summation⁵⁴ for the electrostatic interactions. An energy-based switched cutoff between 9 and 13 Å was employed to truncate the van der Waals interactions.

Each simulation box contained 50 dipeptide molecules in zwitterionic form and 1000 water molecules, matching the composition used in prior experimental investigations.^{37,42} In the three polarizable systems, the dipeptides were dispersed uniformly in the simulation cell and then surrounded with TIP4P-FQ water. The three nonpolarizable systems used the same dipeptide starting structures but were solvated with TIP3P water. To examine the effects of initial geometry, a preclustered Gly-Ala system was also prepared. To generate this structure, the 50 dipeptides were extracted from one of the clustered structures in the nonpolarizable Gly-Ala simulation, and evolved dynamically in vacuum until the system collapsed, at which point it was resolvated with TIP3P water, to obtain a preclustered structure in which the intermolecular contacts are initially favorable. All simulations were run for 38 ns (polarizable) or 200 ns (fixed-charge), under conditions that were identical for all seven systems except for the time step. Simulations of bulk TIP3P and TIP4P-FQ water were also run for 8 and 4 ns, respectively, to obtain properties of bulk water, using systems of 1444 TIP3P or 1440 TIP4P-FQ water molecules.

Hydrogen bonding between dipeptides and water was used to characterize the interaction between the solutes and the solvent. The criteria used to define a hydrogen bond were a hydrogen-to-acceptor distance of 2.4 Å or shorter, and an acceptor–hydrogen–donor angle of 135° or greater. Hydrogen-bond lifetimes were used to characterize the dynamics of these interactions, calculated as the time elapsed between first detection of a hydrogen bond and the first subsequent time at which the hydrogen bond was not present. Mean hydrogen-bond lifetimes were obtained by averaging over all atoms and all hydrogen-bonding events for each atom. The time resolution for individual hydrogen-bond observations was 2 ps.

Solvent and solute dynamics were also characterized using translational diffusion coefficients, which were calculated from the slope of the mean square displacement (MSD) at long times, using the Einstein relation:

$$\lim_{t \rightarrow \infty} \langle |\mathbf{r}(t' + t) - \mathbf{r}(t')|^2 \rangle = 6Dt \quad (1)$$

The diffusion coefficient of water was calculated using the MSD of the oxygen atoms of all water molecules. The diffusion coefficient for the dipeptides was calculated using the MSD of the peptide-bond nitrogen of the second amino acid, which is near the center of mass of each dipeptide.

Rotational reorientation times for water and dipeptides were also used to characterize the dynamics of the system. These were calculated using orientational correlation functions, as obtained from:

$$C(t) = \langle P_2(\boldsymbol{\mu}(t') \cdot \boldsymbol{\mu}(t' + t)) \rangle \quad (2)$$

where P_2 is the second-order Legendre polynomial, and $\boldsymbol{\mu}(t)$ is a unit vector parallel to the molecular dipole moment at time t . Unlike the case for bulk water,¹⁴ these orientational correlation functions are not well described with a single-exponential decay time in the dipeptide solutions. This is consistent with both theoretical predictions of double-exponential decay in orientational relaxation at single binding sites, as well as experimental observations of multiple decay times.^{55,56} Consequently, the orientational correlation functions were fit with a double exponential, resulting in both a slow and a fast decay time, assumed to correspond to the two populations of interfacial and bulk water, respectively.

RESULTS AND DISCUSSION

The polarization of the solvent is measurably perturbed in the concentrated dipeptide solutions, as illustrated by the water dipole moment distributions in Figure 1. As expected, the

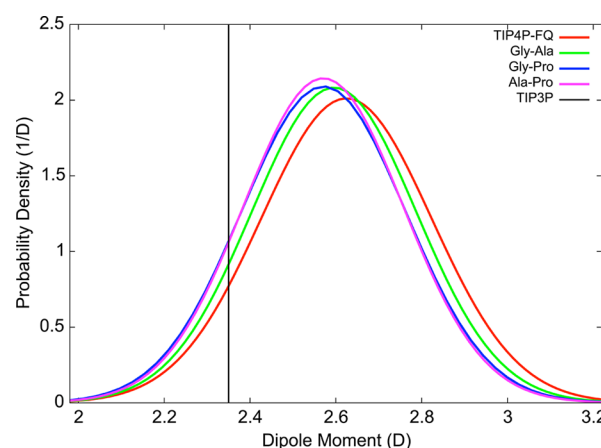


Figure 1. Dipole moment distributions of TIP4P-FQ in the bulk and in solutions of Gly-Ala, Gly-Pro, and Ala-Pro. The fixed dipole moment of TIP3P water is shown for comparison.

polarizable TIP4P-FQ model has a mean dipole moment that is larger than that of the nonpolarizable TIP3P model, and this remains true in the dipeptide solutions. In these solutions, however, the TIP4P-FQ water is depolarized to varying degrees, depending on the hydrophobicity of the dipeptides. In the Gly-Ala solution, the mean induced dipole for water (i.e., the excess over the 1.85 D gas-phase dipole value) is decreased by 5.1% relative to that of pure TIP4P-FQ, while the more hydrophobic Gly-Pro and Ala-Pro solutes caused a larger 6.6% and 7.3% depolarization, respectively. Although fairly small, this depolarization cannot occur in a nonpolarizable simulation and may have effects on the structure and dynamics of the solution.

The choice of force field does affect the structure of the solution, as is evident from the solute–solvent radial distribution functions (rdf's) displayed in Figure 2. In general, the TIP4P-FQ water is more structured around the CHARMM-FQ dipeptides than is TIP3P water around the nonpolarizable CHARMM dipeptides, as illustrated by the elevated rdf in the first and second solvation shells, out to ~8 Å. The force fields differ in their parametrization, in addition to their treatment of polarization, so this difference in solution structure cannot be attributed entirely to the effects of polarization per se. Indeed, it seems likely that the enhanced water structure is a result of stronger interactions with the

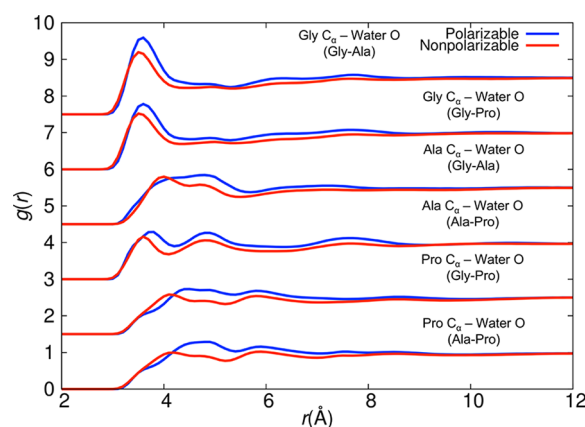


Figure 2. Radial distribution functions for the distance between α carbon atoms for each dipeptide residue and water oxygen atoms, in both polarizable (blue) and nonpolarizable (red) simulations. Curves have been offset along the vertical axis to improve readability.

increased mean dipole moment of the TIP4P-FQ water model, rather than its broader distribution of dipole moments.

The enhanced peptide–water interaction in the polarizable simulations can be seen more directly from an increase in the number of solute–solvent hydrogen bonds. Table 1 shows that

Table 1. Average Number of Hydrogen Bonds (N_H) between Peptide and Water, and the Average Hydrogen-Bond Lifetime (τ) in Each Solution^a

		Gly-Ala	Gly-Pro	Ala-Pro
N_H	TIP4P-FQ	7.21 ± 0.07	5.98 ± 0.06	6.23 ± 0.07
	TIP3P	5.74 ± 0.05	4.99 ± 0.05	5.18 ± 0.08
τ (ps)	TIP4P-FQ	5.38 ± 0.02	4.89 ± 0.02	4.72 ± 0.02
	TIP3P	5.02 ± 0.02	5.64 ± 0.03	6.12 ± 0.03

^aErrors are standard errors of the mean.

20–40% more peptide–water hydrogen bonds are formed in the polarizable simulations than in the nonpolarizable ones. Not surprisingly, the average number of solute–solvent hydrogen bonds generally decreases as the hydrophobicity of peptides increases. Gly-Ala is the least hydrophobic of the three dipeptides, and, as expected, it forms the greatest number of hydrogen bonds with the solvent. Fewer hydrogen bonds are formed with the more hydrophobic proline-containing dipeptides. With between 5 and 7 waters hydrogen bonded to each dipeptide, it is worth pointing out that in these concentrated solutions about 30% of the water molecules are directly hydrogen bonded to a dipeptide (neglecting bridging waters that form two hydrogen bonds). For comparison, roughly two-thirds of the water molecules are within 5 Å of at least one dipeptide.

The presence of the dipeptide solutes also affects the water structure, as shown by the water rdf's in Figures 3 and 4. In both the nonpolarizable and the polarizable simulations, the water structure is perturbed primarily at short distances, with enhanced structure in the first coordination shell. This happens despite the lowering of the dipole moment in the polarizable solution, and may result in large part from waters in the first solvation shell of a dipeptide. At longer distances, the water–water structure reproduces the model-specific bulk behavior in both cases, including the TIP3P model's well-known lack of structure after the first peak. The TIP4P-FQ water structure is

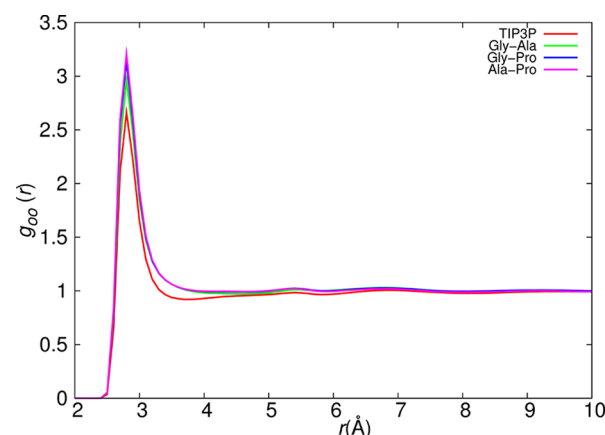


Figure 3. Water O–O radial distribution functions for fixed-charge TIP3P water in pure water and in Gly-Ala, Gly-Pro, and Ala-Pro solutions.

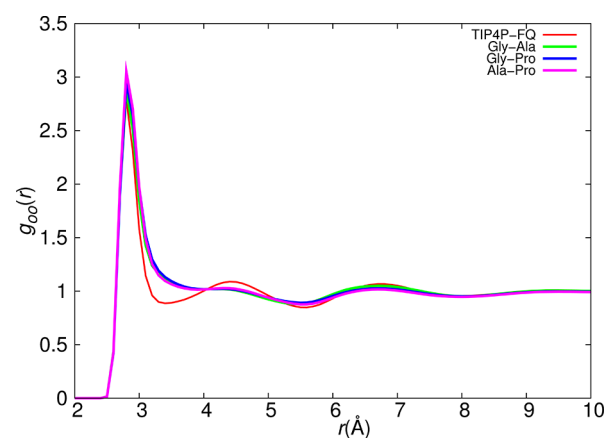


Figure 4. Water O–O radial distribution functions for polarizable TIP4P-FQ water in pure water and in Gly-Ala, Gly-Pro, and Ala-Pro solutions.

generally similar to that of neat TIP4P-FQ, but loses some structure beyond the first shell. The same short-range structuring effect of dipeptides on water is observed in rdf's obtained from neutron diffraction studies,⁴² although the pronounced electrostriction of the second shell observed experimentally is absent here.

The enhanced water structure in the polarizable simulations and increased number of hydrogen bonds in the first solvation shell of the polarizable peptides suggest that there are fewer direct peptide–peptide contacts in the polarizable model. This is indeed the case, as shown by the peptide–peptide rdf's in Figure 5. These all indicate reduced coordination and weaker structure in the polarizable simulations as compared to the fixed-charge simulations. These effects are most pronounced in the first solvation shell, but extend out as far as 12 Å.

Clustering of these dipeptides has been studied by other authors^{37,42} and is of particular interest when these systems are considered as a simple model for aggregation and protein folding. Following McLain et al.,³⁷ we examine the distribution of cluster sizes with two different definitions of clustering. In the first criterion, two molecules are defined to be in the same cluster if the N-terminal hydrogens of one is between 1.5 and 4.5 Å of the C-terminal oxygens of the other. This definition is targeted toward identifying aggregation that is driven by electrostatic or water-mediated hydrophilic interactions. Sim-

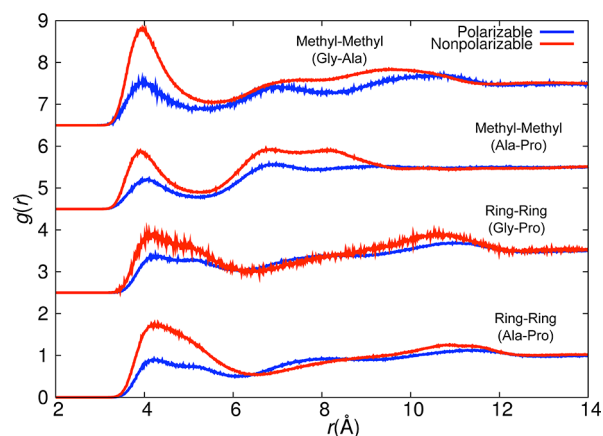


Figure 5. Solute–solute rdf's, evaluated using the methyl–methyl distance (between C_β atoms of each alanine) for alanine-containing dipeptides, and/or the ring–ring distance (between C_γ atoms of the pyrrolidine ring) for proline-containing dipeptides. Curves have been shifted vertically to improve readability.

ilarly, aggregation driven primarily by hydrophobic interactions is identified with a criterion that places molecules in the same cluster when the β carbon atoms of their methyl groups or the γ carbon atoms of their pyrrolidine rings are within 5 Å of one another. Figures 6 and 7 show the distribution of cluster sizes found using these two criteria, for all seven of the dipeptide systems studied, and they reveal several interesting trends.

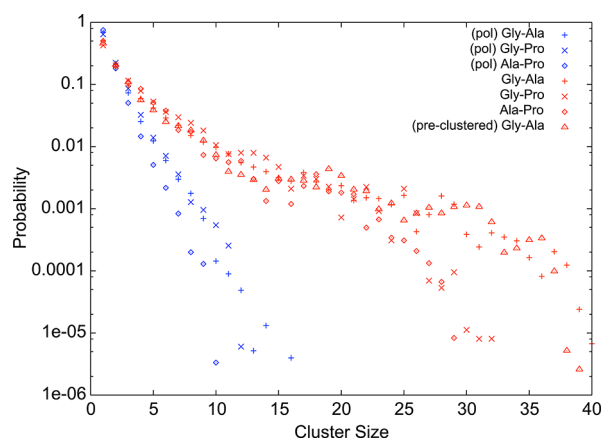


Figure 6. Probability distribution of “hydrophilic” cluster sizes, for all simulations, including the preclustered Gly-Ala solution. Probabilities are calculated as the fraction of clusters with the indicated size, using the hydrophilic contact rule described in the text.

Considering first the nonpolarizable simulations (red points), a comparison of Figure 6 with Figure 7 shows that any clustering is dominated by hydrophilic, rather than hydrophobic, interactions. That is, larger clusters are identified using the hydrophilic contact definition. This agrees with previous modeling by McLain et al.³⁷ Consistent with this observation, the simulations indicate that the least hydrophobic peptide (Gly-Ala) shows the greatest degree of clustering, and the most hydrophobic peptide (Ala-Pro) clusters the least, even when using the hydrophobic criterion. However, the current simulations disagree with previous work in predicting too little association. The clustering probability distributions decay roughly exponentially (approximately linearly on the log scale in Figures 6 and 7), indicating a fairly constant increase in free

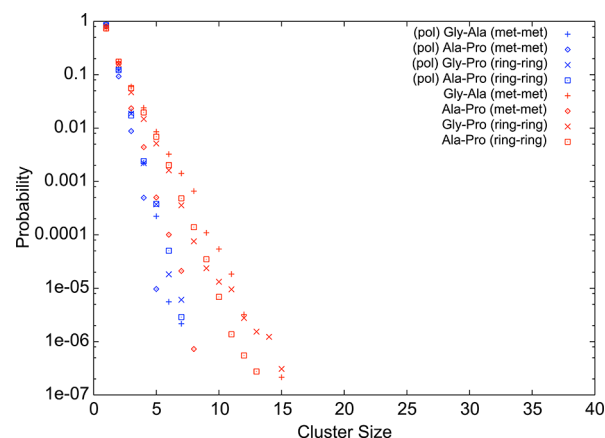


Figure 7. Probability distribution of “hydrophobic” cluster sizes, for all simulations except the preclustered Gly-Ala solution. Probabilities are calculated as the fraction of clusters with the indicated size, using the hydrophobic contact rules described in the text.

energy as each subsequent dipeptide is added to a cluster. Indeed, the relative probabilities of two sequential cluster sizes, P_n and P_{n+1} , can be used to calculate the free energy change upon addition of one dipeptide to a cluster:

$$\Delta G_{n \rightarrow n+1} = -RT \ln \frac{P_{n+1}}{P_n} \quad (3)$$

This average incremental free energy difference is similar for hydrophilic clustering in each system: 0.7 kJ/mol for Gly-Ala and Gly-Pro and 1.0 kJ/mol for Ala-Pro, evaluated over the range $1 \leq n \leq 14$. The free energy cost is higher for cluster growth by hydrophobic contacts, ranging from 2.6 kJ/mol for Gly-Pro to 4.9 kJ/mol for Ala-Pro.

Experimental neutron scattering results, on the other hand, suggest more variation between the different types of dipeptides and indicate that cluster formation is favored in some cases, with larger clusters being more probable than smaller ones.³⁷ Some caution is warranted in directly comparing the structural data from simulation with that inferred from the experimental results (those results also derive in part from atomistic modeling, and there may be many sets of rdf's consistent with the set of diffraction-derived structure factors) but the structures consistent with the experimental results do show strong indications of clustering. In the Gly-Ala solution, for example, 90% of the clusters were predicted to contain 50 molecules or more.³⁷ Single Gly-Ala peptides or dimers were also observed, but the probability of intermediate-size clusters with 5–45 molecules was negligibly small. About 40% of the Gly-Pro dipeptide clusters contained 35 or more molecules, with the rest found primarily as small clusters with 10 or fewer molecules. In other words, these two solutions display behavior typical of nucleation, with a positive free energy cost to add a molecule to a small cluster, but a negative incremental free energy above a critical cluster size. Only the Ala-Pro dipeptide, the most hydrophobic among the three, showed no signs of nucleation in experiment, exhibiting a cluster size distribution that declines monotonically with cluster size, as in the current simulations. Even for that system, however, the simulation underestimates clustering. The average free energy cost for adding a Ala-Pro dipeptide to a cluster is approximately 0.5 kJ/mol if the results of McLain et al.³⁷ are treated as an exponential (with probabilities declining from ~ 0.3 for

monomers to ~ 0.0013 for a 36-molecule cluster). The free energy cost of adding a monomer to a cluster in the present nonpolarizable simulations is about twice as large, 1.0 kJ/mol, resulting in smaller clusters.

To investigate the possibility that larger clusters would be stable in the simulations if they managed to overcome the nucleation barrier, one nonpolarizable Gly-Ala simulation was performed from an initial configuration in which all dipeptides were members of a single cluster, that is, making favorable contacts with each other. The Gly-Ala dipeptide was chosen for this simulation because it showed the greatest degree of aggregation. As can be seen from Figure 6, however, the initial 50-molecule cluster dissociated rapidly, during the 48 ns equilibration period, and the resulting cluster probability distribution is indistinguishable from that obtained from a dispersed starting structure, aside from some small residue of the initial conditions visible at intermediate cluster sizes of 20–40. Thus, if there is a critical nucleation size for a Gly-Ala cluster, it is larger than 50 molecules, in contradiction with the experimental result.

The Gly-Ala system has been studied computationally by Tulip and Bates.⁴³ That study used three different nonpolarizable solvent models (TIP3P, TIP4P, and SPC/E), all with the same CHARMM22 model employed here for the peptide. All three of these models also failed to reproduce the experimentally observed aggregation, predicting a monotonically decreasing probability of clusters with increasing size, and no nucleation barrier, just as with the current simulations. McLain et al. have modeled all three of the dipeptides considered here, using OPLS force field for the peptides and SPC/E for the water model.³⁷ Those simulations did observe hydrophilic clustering of the Gly-Ala dipeptide, with a nucleation barrier at around 20–30 molecules, demonstrating considerably better agreement with experiment. This suggests that the effect of the force field can be quite significant, and that the CHARMM22 force field overestimates the penalty for hydrophilic aggregation.

Turning now to the results from the polarizable model in Figures 6 and 7, it is clear that the polarizable model shows even weaker association between peptides than does the fixed-charge model. The free energy cost of adding a dipeptide to the cluster by hydrophilic contact is similar for each dipeptide, ranging from 2.1 kJ/mol (Gly-Ala) to 3.4 kJ/mol (Ala-Pro), about 3 times as large as the 0.7–1.0 kJ/mol values in the nonpolarizable simulations. These results are consistent with the other structural results: the enhanced water–peptide interactions in the polarizable simulations (Figure 2 and Table 1) decrease peptide–peptide contact, as shown by both the radial distribution functions (Figure 5) and the cluster distributions (Figures 6 and 7), reducing the agreement with experiment. The polarizable CHARMM30 force field was derived from the fixed-charge CHARMM22 model and still shares some of its parameters. It also seems to have inherited that model's tendency toward overpenalizing peptide aggregation, an error that has been exacerbated by the introduction of polarization.

In addition to the structural data, dynamical properties were also analyzed for each dipeptide solution and are presented in Tables 1–3. The lifetimes of hydrogen bonds formed between dipeptides and water (Table 1) are in the vicinity of 5–6 ps, regardless of peptide or model. These lifetimes can be compared to residence times obtained from experimental techniques such as dielectric relaxation,⁵⁷ femtosecond spec-

Table 2. Translational Diffusion Coefficients of Water and Dipeptides

	diffusion coefficient (10^{-5} cm ² /s)				
	water			solute	
	exp. ⁵⁹	TIP4P-FQ	TIP3P	polarizable	fixed-charge
pure water	2.30	2.05	5.54		
Gly-Ala		1.10	2.36	0.15	0.06
Gly-Pro		1.37	2.20	0.17	0.08
Ala-Pro		1.22	1.88	0.09	0.14

troscopy,^{56,58} or quasi-elastic neutron scattering (QENS).³⁹ Experimental data are not available for the dipeptide solutions studied here and differ by as much as an order of magnitude depending on the biomolecular solute in question, but generally range from less than 10 to more than 80 ps. The average residence times observed here are on the short side of this range for both models, suggesting that the water molecules are more weakly bound to these dipeptides than to the tryptophan residues used as a probe in the fluorescence experiments.^{56,58}

The polarizable and nonpolarizable models show opposing trends in the variation of individual hydrogen-bond lifetime with the different peptides. When modeled with the polarizable model, hydrogen-bond lifetimes between water and hydrophilic peptides are longer than those between water and hydrophobic peptides. The opposite is seen in nonpolarizable simulations, however; the hydrogen bonds are longer-lived in the hydrophobic solutions.

These hydrogen-bond lifetimes are close to 5 ps in all systems, so the difference between models is not dramatic. Yet an analysis of the translational and rotational motions reveals that the solvent dynamics are considerably slower for the polarizable model. In the bulk solvent, the self-diffusion coefficient (Table 2) is only 37% as large for TIP4P-FQ water as for TIP3P water, and in much better agreement with experiment.⁵⁹ The same trend persists in the dipeptide solutions, where the water diffusion coefficients (Table 2) are again smaller with the polarizable model than with the nonpolarizable model, consistent with the behavior in pure water.

For both models, the water diffusion is considerably slower in the peptide solutions than in the pure liquid; this is consistent with experimental studies that show slowed translational dynamics for water at the interface of various biomolecular solutes.^{39,56,60} In these systems, interaction with the solute slows diffusion by a factor of 1.5–1.9 in the polarizable model and by 2.3–2.9 in the nonpolarizable model, consistent with magnetic relaxation dispersion⁶⁰ and QENS³⁹ observations that translational diffusion of interfacial water molecules is slowed by a factor of about 2 or 3 in the hydration layer of proteins. The solvent diffusion coefficients of $(1.1\text{--}1.4) \times 10^{-5}$ cm²/s obtained with TIP4P-FQ are in reasonable agreement with the values of $(0.7\text{--}1.1) \times 10^{-5}$ cm²/s obtained for concentrated solutions of different small peptides using QENS.³⁹

The solute diffusivities are much smaller than those for the solvent, due to the larger size of the solute molecules. The polarizable model generally predicts that the largest (and most hydrophobic) Ala-Pro solute diffuses more slowly than the smaller and more hydrophilic Gly-Ala and Gly-Pro, as would be expected. Interestingly, however, the nonpolarizable solutes show the opposite trend: the larger and more hydrophobic dipeptides diffuse more quickly than the smaller and more hydrophilic ones. This is particularly curious, given that the

Table 3. Rotational Reorientation Times (\pm Standard Error) of Bulk and Interfacial Water in Dipeptide Solutions

	τ (ps)						
	water	Gly-Ala		Gly-Pro		Ala-Pro	
		bulk	interfacial	bulk	interfacial	bulk	interfacial
TIP4P-FQ	2.13 ± 0.11	0.59 ± 0.03	6.44 ± 0.16	0.53 ± 0.03	5.53 ± 0.15	0.53 ± 0.03	6.10 ± 0.13
TIP3P	0.69 ± 0.02	1.00 ± 0.02	13.6 ± 0.62	1.16 ± 0.02	36.1 ± 2.19	1.20 ± 0.03	31.3 ± 1.77

water–peptide hydrogen bonds survive longer around hydrophobic solutes than around hydrophilic ones in nonpolarizable solutions (Table 1), which would increase the hydrodynamic radius.

Rotational reorientation times (Table 3) show that TIP4P-FQ water not only translates but also rotates more slowly than TIP3P in the pure liquid. Once again, the TIP4P-FQ model is in reasonable agreement with the experimental value of 1.95 ps,⁶¹ but TIP3P water is too mobile in this case, reorienting about 3 times more quickly than it should. When the dipeptides are added, the decay of the orientational correlation function becomes biexponential (Table 3), with a fast decay time of 0.5 ps (TIP4P-FQ) to 1 ps (TIP3P) and a slower decay time of 5 ps (TIP4P-FQ) to 30 ps (TIP3P). This is consistent with theoretical models and experimental results, which attribute the faster time scale to motion of bulk-like solvent molecules that are not interacting strongly with the solute and the slower time scale to solvent molecules that are bound to the solute.⁵⁶ The time scales vary with the biomolecular solute being studied, but for small proteins the fast time scale is roughly 1 ps and the slower time scale is in the range of 20–50 ps.⁵⁶ Although experimental data are not available for these dipeptides, the TIP3P model is in better agreement with the time scales observed for other biomolecules, while the TIP4P-FQ model exhibits slightly faster dynamics.

CONCLUSION

In this study, three different concentrated aqueous dipeptide solutions were modeled with both a polarizable model (TIP4P-FQ and CHARMM30) and a nonpolarizable model (TIP3P and CHARMM22), analyzing both the structure and the dynamics of these systems to determine the effects of polarization. These concentrated systems, all in excess of 2 M, serve as a useful system to examine such polarization effects, because roughly two-thirds of the solvent molecules are within 5 Å of a solute molecule, and thus experience a perturbed and anisotropic electrostatic environment. The waters in all three solutions were found to be depolarized with the most hydrophobic Ala-Pro solution being affected the most.

The peptide–water interaction was found to be enhanced in polarizable simulations, based on several structural measures. This is likely not a direct effect of polarization, but rather a result of the larger average dipole moment enabled by the polarizable simulation.

Both models predict that the translational diffusion of water is slowed in concentrated peptide solution, relative to neat water. Both models also predict a substantial slowing of the rotational motion of a portion of the solvent in the peptide solutions, attributed to bound water molecules at the biological interface region. The rotational motions of both bulk and interfacial water molecules are faster for the polarizable model than for the nonpolarizable model, by factors of roughly 2–5. On the other hand, the translational dynamics of the polarizable model are slower than those of the nonpolarizable model.

Generally, it is difficult to predict the effect of polarization on dynamical properties: the enhanced dipole allowed by polarizable models generally acts to slow the dynamics, but the ability of the dipole to adjust and lower diffusive barriers then tends to speed up the dynamics.⁶² In this system, apparently, the former effect dominates for translational motion, while the latter effect dominates for rotations.

Neither the polarizable nor the nonpolarizable simulations was able to reproduce the experimentally observed aggregation of the dipeptides. The polarizable model showed less aggregation, consistent with stronger peptide–water interactions, but in poorer agreement with experiment. This can be interpreted as a deficiency of the CHARMM family of models, because simulations with OPLS and SPC/E have exhibited aggregation,³⁷ but current and previous⁴³ simulations with CHARMM and a variety of solvent models have not. Additional studies of aggregation can thus help diagnose and improve these deficiencies, which are expensive to study with full peptide folding simulations; although CHARMM has been used to model the early stages of peptide folding with some success,^{63,64} and seems to work better than AMBER or OPLS-AA for modeling peptide adsorption,⁶⁵ there have been very few simulations of peptide folding using CHARMM in explicit solvent, and there are some known limitations in the folding free energy landscape.^{66,67}

Considering that the TIP4P water model has more realistic water structure and dynamics, the fully polarizable models include physical effects that are absent in the nonpolarizable models, and that this polarization has noticeable effects on dipole distributions, structure, and dynamics in the chosen systems, it is perhaps surprising that the polarizable simulations are not in better agreement with experiment. Although there are a number of possible interpretations for this result, the most likely explanation is the one consistent with all of the observations: that polarization does indeed have the effect of reducing aggregation, but that neither model (nonpolarizable or polarizable) is parametrized sufficiently well to reproduce the experimental results.

The weaker clustering in the polarizable simulations seems to arise because peptide–peptide contacts are diminished in the presence of enhanced peptide–water interactions. Whether these stronger interactions are the result of polarization, per se, or merely the partial reparameterization of the models (including a stronger mean dipole moment on water, for example), is impossible to determine from the current investigations. Decoupling the effects of polarization and parametrization is not impossible, but requires additional tests with specially constrained models.⁸ It seems quite likely, however, that the changes in charge distributions and solvent dynamics are real physical effects induced by depolarization around nonpolar solutes.

The partial failure of both models to accurately describe aggregation is an example of a common problem in parametrizing empirical force fields: models can be parametrized well for simple structural and energetic properties, and

perform poorly on complex, equilibrium properties. Most commonly, peptide force fields are parametrized using pairwise interactions between pairs of molecules, for computational efficiency. The current simulations suggest that biomolecular force fields, particularly polarizable ones, could benefit from fitting to ensemble-averaged interactions (e.g., free energies or liquid structure) in fully solvated environments that mimic the applications for which they will be used.

The dipeptide simulations prove to be a valuable test case for aqueous biomolecular modeling: any flaws that lead to inadequate description of dipeptide clustering, perhaps due to incorrect peptide–water interactions, will also have consequences in more complex processes such as protein folding, protein–protein interactions, and aggregation of larger peptides. Thus, a detailed understanding of peptide aggregation from these and other studies will be valuable not only for the study of concentrated dipeptide solutions, but also for many biological processes.

AUTHOR INFORMATION

Corresponding Author

*E-mail: ss@clemson.edu.

Notes

The authors declare no competing financial interest.

ACKNOWLEDGMENTS

We gratefully acknowledge financial support from the DoD (47539-CH-MUR) and computational support by the Clemson CITI staff.

REFERENCES

- (1) Cieplak, P.; Dupradeau, F.-Y.; Duan, Y.; Wang, J. J. *Phys. Cond. Matt.* **2009**, *21*, 333102.
- (2) Vorobyov, I.; Anisimov, V. M.; Greene, S.; Venable, R. M.; Moser, A.; Pastor, R. W.; MacKerell, A. D., Jr. *J. Chem. Theory Comput.* **2007**, *3*, 1120–1133.
- (3) Illingworth, C. J.; Domene, C. *Proc. R. Soc. A* **2009**, *465*, 1701–1716.
- (4) Allen, T. W.; Bastug, T.; Kuyucak, S.; Chung, S. H. *Biophys. J.* **2003**, *84*, 2159–2168.
- (5) Bastug, T.; Kuyucak, S. *Chem. Phys. Lett.* **2006**, *424*, 82–85.
- (6) Bastug, T.; Kuyucak, S. *Biophys. J.* **2006**, *90*, 3941–3950.
- (7) Illingworth, C. J. R.; Furini, S.; Domene, C. *J. Chem. Theory Comput.* **2010**, *6*, 3780–3792.
- (8) Stuart, S. J.; Berne, B. J. *J. Phys. Chem.* **1996**, *100*, 11934–11943.
- (9) Stuart, S. J.; Berne, B. J. *J. Phys. Chem. A* **1999**, *103*, 10300–10307.
- (10) Halgren, T. A.; Damm, W. *Curr. Opin. Struct. Biol.* **2001**, *11*, 236–242.
- (11) Wei, C.; Tung, D.; Yip, Y. M.; Mei, Y.; Zhang, D. *J. Chem. Phys.* **2011**, *134*, 171101.
- (12) Rick, S. W.; Stuart, S. J. *Rev. Comput. Chem.* **2002**, *18*, 89–146.
- (13) Rick, S. W.; Stuart, S. J.; Bader, J. S.; Berne, B. J. *J. Mol. Liq.* **1995**, *65–6*, 31–40.
- (14) Rick, S. W.; Stuart, S. J.; Berne, B. J. *J. Chem. Phys.* **1994**, *101*, 6141–6156.
- (15) Davis, J. E.; Patel, S. J. *J. Phys. Chem. B* **2009**, *113*, 9183–9196.
- (16) Davis, J. E.; Raharnan, O.; Patel, S. *Biophys. J.* **2009**, *96*, 385–402.
- (17) Patel, S.; Brooks, C. L. *Mol. Simul.* **2006**, *32*, 231–249.
- (18) Patel, S.; Brooks, C. L. *J. Comput. Chem.* **2004**, *25*, 1–15.
- (19) Patel, S.; Mackerell, A. D.; Brooks, C. L. *J. Comput. Chem.* **2004**, *25*, 1504–1514.
- (20) Ren, P. Y.; Ponder, J. W. *J. Phys. Chem. B* **2003**, *107*, 5933–5947.
- (21) Ren, P. Y.; Ponder, J. W. *J. Comput. Chem.* **2002**, *23*, 1497–1506.
- (22) Lamoureux, G.; Harder, E.; Vorobyov, I. V.; Roux, B.; MacKerell, A. D. *Chem. Phys. Lett.* **2006**, *418*, 245–249.
- (23) Lamoureux, G.; Roux, B. *J. Chem. Phys.* **2003**, *119*, 3025–3039.
- (24) Lopes, P. E. M.; Lamoureux, G.; Mackerell, A. D., Jr. *J. Comput. Chem.* **2009**, *30*, 1821–1838.
- (25) Lopes, P. E. M.; Lamoureux, G.; Roux, B.; MacKerell, A. D., Jr. *J. Phys. Chem. B* **2007**, *111*, 2873–2885.
- (26) Yu, H.; Whitfield, T. W.; Harder, E.; Lamoureux, G.; Vorobyov, I.; Anisimov, V. M.; MacKerell, A. D., Jr.; Roux, B. *J. Chem. Theory Comput.* **2010**, *6*, 774–786.
- (27) Grossfield, A.; Ren, P. Y.; Ponder, J. W. *J. Am. Chem. Soc.* **2003**, *125*, 15671–15682.
- (28) Kaminski, G. A.; Friesner, R. A.; Zhou, R. H. *J. Comput. Chem.* **2003**, *24*, 267–276.
- (29) Kaminski, G. A.; Stern, H. A.; Berne, B. J.; Friesner, R. A.; Cao, Y. X. X.; Murphy, R. B.; Zhou, R. H.; Halgren, T. A. *J. Comput. Chem.* **2002**, *23*, 1515–1531.
- (30) Warshel, A.; Kato, M.; Pislakov, A. V. *J. Chem. Theory Comput.* **2007**, *3*, 2034–2045.
- (31) Lopes, P. E.; Roux, B.; Mackerell, A. D. *Theor. Chem. Acc.* **2009**, *124*, 11–28.
- (32) Ponder, J. W.; Wu, C.; Ren, P.; Pande, V. S.; Chodera, J. D.; Schnieders, M. J.; Haque, I.; Mobley, D. L.; Lambrecht, D. S.; DiStasio, R. A., Jr.; et al. *J. Phys. Chem. B* **2010**, *114*, 2549–2564.
- (33) Geerke, D. P.; van Gunsteren, W. F. *J. Chem. Theory Comput.* **2007**, *3*, 2128–2137.
- (34) Wang, Z. X.; Zhang, W.; Wu, C.; Lei, H. X.; Cieplak, P.; Duan, Y. *J. Comput. Chem.* **2006**, *27*, 781–790.
- (35) Malardier-Jugroot, C.; Johnson, M. E.; Murarka, R. K.; Head-Gordon, T. *Phys. Chem. Chem. Phys.* **2008**, *10*, 4903–4908.
- (36) Johnson, M. E.; Malardier-Jugroot, C.; Murarka, R. K.; Head-Gordon, T. *J. Phys. Chem. B* **2008**, *113*, 4082–4092.
- (37) McLain, S. E.; Soper, A. K.; Daidone, I.; Smith, J. C.; Watts, A. *Angew. Chem., Int. Ed.* **2008**, *47*, 9059–9062.
- (38) Russo, D.; Ollivier, J.; Teixeira, J. *Phys. Chem. Chem. Phys.* **2008**, *10*, 4968–4974.
- (39) Russo, D.; Murarka, R. K.; Copley, J. R. D.; Head-Gordon, T. *J. Phys. Chem. B* **2005**, *109*, 12966–12975.
- (40) Ball, P. *Chem. Rev.* **2008**, *108*, 74–108.
- (41) Nakagawa, H.; Kamikubo, H.; Kataoka, M. *Biochim. Biophys. Acta, Proteins Proteomics* **2010**, *1804*, 27–33.
- (42) McLain, S. E.; Soper, A. K.; Watts, A. *Eur. Biophys. J.* **2008**, *37*, 647–655.
- (43) Tulip, P. R.; Bates, S. P. *J. Chem. Phys.* **2009**, *131*, 015103.
- (44) MacKerell, A. D., Jr.; Bashford, D.; Bellott, M.; Dunbrack, R. L.; Evanseck, J. D.; Field, M. J.; Fischer, S.; Gao, J.; Guo, H.; Ha, S.; et al. *J. Phys. Chem. B* **1998**, *102*, 3586–3616.
- (45) Jorgensen, W. L.; Chandrasekhar, J.; Madura, J. D.; Impey, R. W.; Klein, M. L. *J. Chem. Phys.* **1983**, *79*, 926–935.
- (46) Jorgensen, W. L. *J. Chem. Phys.* **1982**, *77*, 4156–4163.
- (47) Brooks, B. R.; Brooks, C. L., III; MacKerell, A. D., Jr.; Nilsson, L.; Petrella, R. J.; Roux, B.; Won, Y.; Archontis, G.; Bartels, C.; Boresch, S.; et al. *J. Comput. Chem.* **2009**, *30*, 1545–1614.
- (48) MacKerell, A. D., Jr.; Feig, M.; Brooks, C. L., III. *J. Am. Chem. Soc.* **2004**, *126*, 698–699.
- (49) MacKerell, A. D., Jr.; Feig, M.; Brooks, C. L., III. *J. Comput. Chem.* **2004**, *25*, 1400–1415.
- (50) Nose, S. *Mol. Phys.* **1984**, *52*, 255–268.
- (51) Nose, S.; Klein, M. L. *Mol. Phys.* **1983**, *50*, 1055–1076.
- (52) Feller, S. E.; Zhang, Y. H.; Pastor, R. W.; Brooks, B. R. *J. Chem. Phys.* **1995**, *103*, 4613–4621.
- (53) Ryckaert, J. P.; Cicciotti, G.; Berendsen, H. J. C. *J. Comput. Phys.* **1977**, *23*, 327–341.
- (54) Darden, T.; York, D.; Pedersen, L. *J. Chem. Phys.* **1993**, *98*, 10089–10092.
- (55) Nandi, N.; Bagchi, B. *J. Phys. Chem. B* **1997**, *101*, 10954–10961.

- (56) Pal, S. K.; Peon, J.; Bagchi, B.; Zewail, A. H. *J. Phys. Chem. B* **2002**, *106*, 12376–12395.
- (57) Pethig, R. *Annu. Rev. Phys. Chem.* **1992**, *43*, 177–205.
- (58) Li, T.; Hassanali, A. A.; Kao, Y.-T.; Zhong, D.; Singer, S. J. *J. Am. Chem. Soc.* **2007**, *129*, 3376–3382.
- (59) Krynicky, K.; Green, C.; Sawyer, D. *Faraday Discuss.* **1978**, *66*, 199–208.
- (60) Modig, K.; Liepinsh, E.; Otting, G.; Halle, B. *J. Am. Chem. Soc.* **2004**, *126*, 102–114.
- (61) Ludwig, R.; Weinhold, F.; Farrar, T. C. *J. Chem. Phys.* **1995**, *103*, 6941–6950.
- (62) Rick, S. W.; Stuart, S. J. *Rev. Comput. Chem.* **2002**, *18*, 89–146.
- (63) Yeh, I.-C.; Hummer, G. *J. Am. Chem. Soc.* **2002**, *124*, 6563–6568.
- (64) Kent, A.; Jha, A. K.; Fitzgerald, J. E.; Freed, K. F. *J. Phys. Chem. B* **2008**, *112*, 6175–6186.
- (65) Collier, G.; Vellore, N. A.; Yancey, J. A.; Stuart, S. J.; Latour, R. A. *Biointerphases* **2012**, *7*, 24.
- (66) Freddolino, P. L.; Park, S.; Roux, B.; Schulten, K. *Biophys. J.* **2009**, *96*, 3772–3780.
- (67) Freddolino, P. L.; Harrison, C. B.; Liu, Y.; Schulten, K. *Nat. Phys.* **2010**, *10*, 751–758.